



HAL
open science

Luminescence-Sensitive Surfaces Bearing Ratiometric Nanoparticles for Bacteria Growth Detection

Miaobo Pan, Gabriela Morán Cruz, Chloé Grazon, Djamila Kechkeche, Ludivine Houel Renault, Gilles Clavier, Rachel Méallet-Renault

► **To cite this version:**

Miaobo Pan, Gabriela Morán Cruz, Chloé Grazon, Djamila Kechkeche, Ludivine Houel Renault, et al.. Luminescence-Sensitive Surfaces Bearing Ratiometric Nanoparticles for Bacteria Growth Detection. ACS Applied Polymer Materials, 2022, 4 (8), pp.5482-5492. 10.1021/acsapm.2c00549 . hal-03789930

HAL Id: hal-03789930

<https://hal.science/hal-03789930>

Submitted on 27 Sep 2022

HAL is a multi-disciplinary open access archive for the deposit and dissemination of scientific research documents, whether they are published or not. The documents may come from teaching and research institutions in France or abroad, or from public or private research centers.

L'archive ouverte pluridisciplinaire **HAL**, est destinée au dépôt et à la diffusion de documents scientifiques de niveau recherche, publiés ou non, émanant des établissements d'enseignement et de recherche français ou étrangers, des laboratoires publics ou privés.

Luminescent sensitive surfaces bearing ratiometric nanoparticles for bacteria growth detection

Miaobo Pan¹, Gabriela Moran¹, Chloé Grazon^{2,3}, Djamila Kechkeche², Ludivine Houel Renault¹, Gilles Clavier², Rachel Méallet-Renault^{1}*

¹ Université Paris-Saclay, Institut des Sciences Moléculaires d'Orsay (ISMO), CNRS, 91400, Orsay, France

² Université Paris-Saclay, ENS Paris-Saclay, CNRS, PPSM, 91190, Gif-sur-Yvette, France

³ Université Bordeaux, CNRS, Bordeaux INP, ISM, UMR 5255, F-33400 Talence, France

*Corresponding author:

Rachel Méallet-Renault

Tel: +33169153128/+33671124932

E-mail : rachel.meallet-renault@universite-paris-saclay.fr

Current address : Université Paris-Saclay, Institut des Sciences Moléculaires d'Orsay (ISMO), CNRS, 91400, Orsay, France

KEYWORDS Polymer nanoparticle; fluorescent; ratiometric; pH measurement; glass surface

ABSTRACT pH is one of the most fundamental parameters to describe the quality of aqueous solutions. We developed a ratiometric fluorescent platform to monitor pH not only in solution but also on surfaces: our nanoprobe is based on fluorescent nanoparticles (FNPs) with a red-emitting BODIPY (red-BDPMA) core and a pH-sensitive fluorescein derivative grafted on the outer shell. We demonstrated that a limited but controlled Förster Resonant Energy Transfer (FRET) occurs between the two fluorophores. Such pH-sensitive and ratiometric FNP could be grafted on a

silanized glass surface and still permitted to measure pH with a good sensitivity and allowed the monitoring of *E. coli* growth through optical measurement under physiological pH range.

Introduction

pH is one of the most fundamental parameters to describe the quality of aqueous solution. The determination of pH is inevitable across a wide range of fields, from environmental to biomedicine and industry. pH is one of the key values to be measured in drinking water¹, biochemistry^{2,3}, medicine^{4,5}, food and beverage industries^{6,7} and industrial waste applications⁸. The global pH sensor market kept growing during the past decades showing that there is a strong demand.

There are a number of methods to measure the pH of a solution. The most widely used are pH paper, electrochemical or electrical methods and optical ones. Electrochemical and electrical methods are mainly ion-sensitive field effect transistors (ISFET⁹), glass electrodes or modified electrodes with polymers¹⁰. However, the electrodes are difficult to miniaturize and sensitive to extraneous influences. The electrodes obviously cannot be applied to sense pH values on a nanometer scale, such as inside cells. Many of these problems can be well overcome by optical methods and imaging technologies, which have achieved increasingly attractive progress in sensitivity and have the great advantage of being non-invasive¹¹. Recently many luminescent pH nanomaterial-based probes have been developed and widely applied in various fields¹². Several recent review papers discuss organic-based nanomaterials for pH measurement^{13–16}. Among those nanomaterials, the dye-doped ones are widely used. Multiple dyes attached to or embedded in nanoparticles, not only lead to dramatically enhanced brightness and stability but also improve the signal contrast. This kind of nanoprobe are well suited for the determination of pH in several microenvironments (such as cells or biological tissues)^{17–20}. Organic-based nanomaterial sensors

are very attractive because they make intracellular pH determination feasible, with improved sensitivity, more selective targeting, higher specificity and greater stability.

The most commonly used pH-sensitive fluorescent dyes are fluorescein and its derivatives, benzoxanthene dyes and cyanine based stains^{21,22}. Fluorescein various protolytic forms in aqueous solution (cationic, neutral, anionic and dianionic) make its absorption and fluorescence properties strongly pH-dependent. Around neutral domain, fluorescein has an intense fluorescence with a high quantum yield²³ which is fully effective at physiological condition (pH~7.3). Moreover, several reactive fluorescein derivatives are commercially available which leads to their high popularity in biological applications²⁴.

Dyes with boron dipyrromethene (BODIPY) core are famous for their versatility and they are widely applied in fluorescent sensing and imaging^{25,26}. BODIPY is reasonably stable due to its insensitivity to the polarity and surrounding pH conditions²⁷. Furthermore, to achieve tunable emission characteristics, the BODIPY core can be modified and extended through various functional groups^{28,29}. In former works, our group designed a green-BODIPY derivative with a polymerizable group (methacrylate) that could be covalently incorporated in the polystyrene core of the NPs to design bright fluorescent nanoparticles (FNPs). Fluoresceinamine was grafted to the shell of the nanoparticles to obtain an ultra-bright ratiometric pH sensor³⁰. Emission bands of fluoresceinamide (FAM) and BODIPY could be detected. They were too close (515 and 547nm, respectively) for practical use and to demonstrate Förster resonance energy transfer (FRET) mechanism in between those two yellow-green emitting dyes. In order to investigate the possible modulation of the nature of the copolymerized BODIPY dye and to avoid too large overlap between the fluorescence spectra of the FRET pair, we designed a red-emitting dye compatible with fluorescein that could be included in the core of the NPs.

Thus a naphthalene-methacrylate BODIPY derivative (red-BDPMA) with longer absorption and emission wavelengths than the green one previously used, is introduced to design FNP_{Red} as a fluorescent platform. Such FNP_{Red} are more suited for *in vivo* imaging since they are excited and emit above 550 nm. To elaborate nanoparticles with dual emission, the pH-sensitive fluorescein dye was grafted on the FNP_{Red} shell by peptide coupling to obtain the FNP_{Red-FA} particles.

Moreover, if sensing is done with NPs in suspension, imaging requires multiple steps such as centrifugation and deposition prior to observation. Immobilization of the nanosensor on a surface allows overcoming these difficulties. Glass is one of the most ideal materials due to its excellent transparency and good compatibility with a variety of solvents and reagents, besides its wide use in microscopy and biocompatibility. The high density of hydroxyl groups on the glass surface makes functionalization easy and efficient through silane-coupling. It is thus widely used in the elaboration of devices such as microchips.

In this work, we covalently immobilized the biocompatible, bright ratiometric FNP_{Red-FA} onto glass slides to avoid leakage and to ease pH monitoring. The ratio of the two dyes' fluorescence intensity is sensitive to pH in the physiological range (pH 5.0 to 7.6). Additionally, this surface allowed for rapid and continuous monitoring of *Escherichia coli* (*E. coli*) growth. To the best of our knowledge, it is the first demonstration that a glass slide grafted with pH-sensitive FNPs succeeded in the detection of bacteria growth by ratiometric fluorescence measurement.

EXPERIMENTAL SECTION

Materials

Commercially available reagents were used without further purification unless otherwise stated. 1-methylnaphthalene (C₁₁H₁₀, CAS: 90-12-0, MW: 142.20), butyryl chloride (C₄H₇OCl, CAS:

141-75-3, MW: 106.55), aluminum trichloride (AlCl_3 , CAS: 7446-70-0, MW: 133.34), hydroxylamine hydrochloride (NH_4OCl , CAS: 5470-11-1, MW: 69.49), mercury acetate ($\text{C}_4\text{H}_6\text{O}_4\text{Hg}$, CAS: 1600-27-7, MW: 318.68), sodium borohydride (NaBH_4 , CAS: 16940-66-2, MW: 37.83), 4-hydroxybenzaldehyde ($\text{C}_7\text{H}_6\text{O}_2$, CAS: 123-08-0, MW: 122.12), chloranil ($\text{C}_6\text{Cl}_4\text{O}_2$, CAS: 118-75-2, MW: 245.88), *N,N*-diisopropyl-*N*-ethylamine ($\text{C}_8\text{H}_{19}\text{N}$, CAS: 7087-68-5, MW: 129.24), boron trifluoride diethyletherate ($\text{C}_4\text{H}_{10}\text{OBF}_3$, CAS: 109-63-7, MW: 141.93), 1,8-diazabicyclo[5.4.0]undec-7-ene ($\text{C}_9\text{H}_{16}\text{N}_2$, CAS: 6674-22-2, MW: 152.24), methacryloyl chloride ($\text{C}_4\text{H}_5\text{ClO}$, CAS: 920-46-7, MW: 104.53) were used after distillation, acrylic acid (AA, $\text{C}_3\text{H}_4\text{O}_2$, CAS: 79-10-7, MW: 72.06), poly(ethylene glycol) methyl ether acrylate (average Mn 480), 2-methyl-2-[(dodecylsulfanylthiocarbonyl)sulfanyl]propanoic acid (TTCA, $\text{C}_{17}\text{H}_{32}\text{O}_2\text{S}_3$, CAS: 461642-78-4, MW: 364.63) and styrene (C_8H_8 , CAS: 100-42-5, MW: 104.15) were purchased from Merck, Strem or TCI. EDSA (3-(Ethoxydimethylsilyl) propylamine) was purchased from Fluorochem Ltd. Absolute ethanol (L.R.) was purchased from Fisher Scientific. Acetone, ethanol 96% vol. were purchased from VWR. Sulfuric acid 95%, hydrogen peroxide 30%, EDC (*N*-(3-Dimethylaminopropyl)-*N'*-ethylcarbodiimide hydrochloride, $\text{C}_8\text{H}_{17}\text{N}_3\cdot\text{HCl}$, CAS: 25952-53-8, MW: 191.70) and Fluoresceinamine, isomer I ($\text{C}_{20}\text{H}_{13}\text{NO}_5$, CAS: 3326-34-9, MW: 347.32g/mol), Acetyl chloride (CH_3COCl , CAS: 75-36-5, MW: 78.50) were purchased from Sigma Aldrich.

For buffer preparation, sodium phosphate monobasic dihydrate ($\text{NaH}_2\text{PO}_4\cdot 2\text{H}_2\text{O}$, CAS: 13472-35-0, MW: 156.01g/mol), sodium phosphate dibasic dihydrate ($\text{Na}_2\text{HPO}_4\cdot 2\text{H}_2\text{O}$, CAS: 10028-24-7, MW: 177.99g/mol), and anhydrous citric acid ($\text{C}_6\text{H}_8\text{O}_7$, CAS: 77-92-9, MW: 192.12g/mol) were purchased from Sigma Aldrich. Fluorescein disodium salt (CAS: 518-47-8, MW: 376.27g/mol), Sulforhodamine 101 free acid (CAS: 60311-02-6, MW: 606.71g/mol), Rhodamine 590 chloride

(CAS: 989-38-8, MW: 479.0g/mol) were purchased from Exciton. Ultrapure water (Mili-Q, 18M Ω cm) was used for the preparations of aqueous solutions and all rinses.

Glass slides of 19 mm diameter and 1.5mm thickness were purchased from Agar Scientific(UK). Vivaflow 200 Laboratory Cross Flow Cassette was purchased from Sartorius Stedim Biotech.

Trypase Soy Broth (TSB) was purchased from bioMérieux France, M9 minimal Salts (5X) were purchased from Sigma Aldrich. Live *Escherichia* (*E. coli*, BW25113) were used for the bacterial growth experiments. Bacteria were prepared overnight from stock cultures inoculated in Tryptone Soy Broth (TSB) growth medium. The overnight culture of bacteria was diluted in the modified M9 medium (detail composition of the modified M9 medium given in SI).

Synthesis

Fluoresceinamide (C₂₂H₁₅NO₆, MW: 389.36g/mol) was synthesized as described in literature³¹. Synthesis and characterization of the red-BDPMA are detailed in the Supplementary Information. The copolymerization process of red-BDPMA and styrene to form the red-emitting fluorescent nanoparticles (FNP_{Red}) is based on previous reports^{32–34} and described in details in the SI.

Functionalization of nanoparticles with FA

1mL of FNP_{Red} stock solution (about 2.6x10¹⁵ particles/mL) was diluted with pH 8.0 citrate-phosphate buffer (0.1M), mixed with FA (1eq., 2.88 μ mol, 1mg). EDC·HCl (4.5eq., 13 μ mol, 2.5mg) was added to the previous mixture, stirred at 4°C overnight. Then a mixture of free FA and FA grafted FNP_{Red} was obtained. The suspension was purified and concentrated with Viva Flow Filtration for 12h to get rid of all un-grafted FA. This FNP_{Red-FA} stock solution was then stored in dark.

Silanization of glass and FNPs Immobilization

Glass slides were first cleaned with acetone, ethanol 96% vol and deionized water (D.I.) and then placed in a homemade Teflon slide-holder and soaked for 20 minutes in a fresh piranha solution (1:1, H₂O₂ 30%: H₂SO₄ 95%). Slides were then taken out from the piranha solution and rinsed thoroughly with D.I. water. Subsequently, the slides were soaked in absolute ethanol for 15 minutes and dried one by one with nitrogen flux (N₂). The slides were exposed overnight at 80°C to 0.2 mL of 3-ethoxydimethylsilylpropylamine (EDSA) for silanization by vapor deposition^{35,36}. Soxhlet extraction was run with acetone as a solvent for a minimum of 3 cycles to remove all free silane from surfaces.

NPs Immobilization

A FNP_{Red-FA} solution was prepared by mixing 200 μL of FNP_{Red-FA} stock solution (about 2.3x10¹⁵ particles/mL), 2.5 mL of pH 8.0 citrate-phosphate buffer (0.1M) with EDC·HCl coupling agent (40eq., 0.21mmol, 40.3 mg) estimated to the acrylic acid units of the FNP introduced during the FNP synthesis. 300 μL of this solution was deposited on each slide and then transferred to a refrigerating chamber set at 4.0°C, letting the reaction run for two hours. Then, slides were washed with a basic (pH=8~10) solution to remove all the un-grafted FNPs adsorbed on the surface then rinsed with D.I water and dried with N₂ flux.

Characterization techniques

NMR: ¹H, ¹³C, ¹⁹F, ¹¹B NMR spectra were recorded in CDCl₃ on a JEOL ECS (400 MHz) spectrometer. All chemical shifts were referenced to Me₄Si (TMS).

High resolution mass spectrometry was performed by the analytical platform of the ICNS laboratory (Gif-sur-Yvette, France).

pH measurements in solution were done with an Orion Star A111 pH meter (Thermo Scientific).

The average hydrodynamic diameter of the nanoparticles was determined by dynamic light scattering (DLS, VascoFlex™ Cordouan Technologies). Stock solutions were diluted to 2.0 mL using filtered deionized (D.I.) water to achieve a concentration of 0.01% in weight. Nanoparticles tracking analysis (NTA) was done by using NS300 Nanosite Malvern Panalytical ($\lambda = 405\text{nm}$ at RT). The light scattered by the diluted suspension of particles and the motion of the particles were captured by a sCMOS camera at 30 frames/s. Three consecutive measures were performed for each sample.

UV-visible spectra were recorded on a UV-2600 spectrometer (Shimadzu Scientific Instruments, Japan). Spectra were recorded either with double-beam configuration in cuvettes (10mm path quartz cell from Hellma, France) or an integrating sphere, ISR-2600. Excitation and emission spectra were measured on a FluoroMax-4 Spectrofluorometer (Horiba Jobin-Yvon), slit's size and scan speed were adjusted in order to have optimal signal-to-noise ratio. Spectra are corrected from apparatus response function (IRF) and lamp fluctuations. For solution and suspension, absorbance was checked to be lower than 0.1 to avoid inner filter effects.

X-Ray Photoelectron Spectroscopy (XPS) was performed on a K Alpha spectrometer from ThermoFisher, equipped with a monochromated X-ray Source ($\text{Al K}\alpha$, 1486.6 eV) with a spot size of 400 μm . At least 4 different zones from a minimum of 2 samples were analyzed for each type of surface. The data treatment was performed with Casa XPS software (Casa Software Ltd., UK). C1s component was set to the binding energy of 284.8eV, by default, which is comes from carbon-carbon and carbon-hydrogen [C-(C, H)] bonds. The peaks were decomposed using a linear baseline, and a component shape defined by the product of a Gauss and a Lorentz function, in the 70:30 ratio. Molar concentration ratios were calculated using peak areas normalized according to Scofield factors. Elements like B, K, C, N, O, F were taken into consideration.

Atomic force microscopy (AFM) studies were performed using a Nanowizard 3 AFM head (JPK Instruments AG, Germany) coupled to a commercial inverted microscope (Axio Observer Z1, Carl Zeiss, Germany). AFM data were acquired using high-speed force spectroscopic mode (Quantitative Imaging mode, JPK). Scanning Electron Microscopy (SEM) was carried out using a scanning electron microscope ZEISS Sigma HD (FEG-SEM) operating at 1 kV (Field Electron Gun to be observed at low voltage to limit the destruction of organic molecules with low energy e-beam). The EBSD step size was 0.1 μm and the EBSD data acquisition and analysis were undertaken using the TSL Orientation Imaging Microscopy, OIMTM software.

Fluorescence intensity and spectral images were recorded with a Leica TCS SP5-AOBS confocal laser scanning microscope. A \times 63 – 1.4 numerical aperture plan apochromat oil immersion objective and 488nm laser excitation were chosen.

Results and discussion

These FNPs are based on a core-shell structure, together forming a kinetically frozen micelle. As represented in **Figure 1**: the core is made of a statistical copolymer of styrene and red-BDPMA, while the shell consists of a statistical copolymer comprising poly-(ethylene oxide) acrylate (PEOA) and acrylic acid (AA). The FNPs were prepared by one-pot reversible addition–fragmentation chain-transfer (RAFT) miniemulsion polymerization using the hydrophilic copolymer as both a RAFT agent and a stabilizing group^{32,33}.

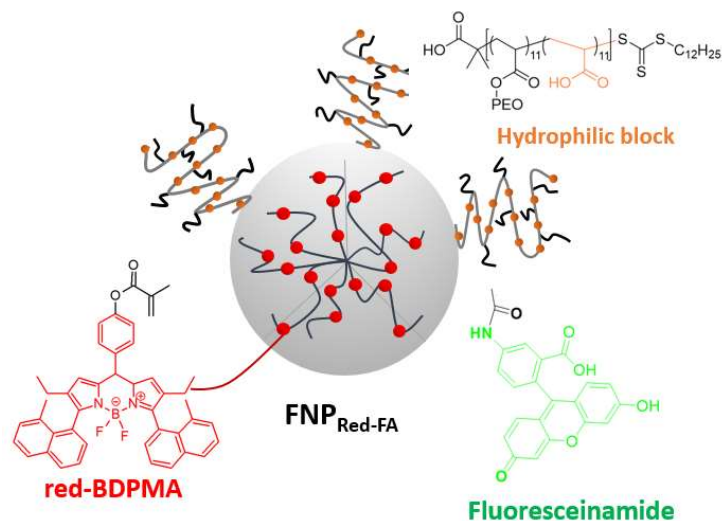


Figure 1. Design of the core-shell FNPs. Core: a statistical copolymer of styrene and red-BODIPY-methacrylate (red-BDPMA); Shell: a random copolymer of poly-(ethylene oxide) acrylate (PEOA) and acrylic acid (AA). The hydrophilic and hydrophobic block form together an amphiphilic block copolymer that assemble in water into a kinetically frozen micelle.

Synthesis and Spectroscopic characterization of the FNPs

The red-emitting BODIPY derivate, red-BDMPA, was prepared following a method previously developed in our group. First a pyrrole substituted by 1-methylnaphthyl and ethyl in positions 2 and 3 respectively was prepared in three steps by the Trofimov reaction³⁷ that involves the reaction of acetylene with the appropriate oxime in super basic media (**Scheme S1**, details in SI). The pyrrole **5** was isolated in a 44% overall yield. BODIPY **7** was then synthesized following standard procedure with 2 equivalents of **5** and one of *p*-hydroxybenzaldehyde in 28% yield. Finally, red-BDPMA **8** was prepared by esterification with methacryloyl chloride in 88% yield (**Scheme S2**).

The fluorescent nanoparticles were synthesized by a one-pot miniemulsion phase inversion process with styrene and red-BDPMA as previously reported by our group^{30,32–34}. We selected the

randomly distributed poly((ethylene oxide) methyl ether acrylate-co-acrylic acid) with a terminal trithiocarbonate (TTC) to act as both the reversible addition-fragmentation transfer (RAFT) copolymerization agent and hydrophilic block (**Scheme S3**). The red-BDPMA with a methacrylate polymerizable function was covalently linked to the styrene polymer chains for the first time to form FNP_{Red}. About 3.2 red-BDPMA monomers per polymer chain could be estimated on average.

FNP_{Red} contain carboxylic acid groups in the shell providing the handle for post-functionalization with amine molecules and the preparation of ratiometric nanosensors. EDC coupling was chosen to graft FA³⁸. It has been shown that excess of EDC (at least two folds) is sufficient to perform grafting of terminal amine function on carboxylic acid groups³⁰.

Thus similar experimental conditions were adopted. The functionalization of the FNP_{Red} with fluoresceinamine was carried out at pH=8.0 and 4°C leading to FNP_{Red-FA} suspension.

FNP_{Red} and FNP_{Red-FA} characteristics are described in **Table 1**. NTA measurements show the same hydrodynamic diameter (70nm), indicating that FA grafting does not affect the particle's size.

Absorption and fluorescence emission spectra of the red-BDPMA recorded in toluene are shown in **Figure S1** and spectroscopic properties are given in **Table 1**. red-BDPMA has an absorption maximum at 558nm, a fluorescence emission maximum at 600nm, and a fluorescence quantum yield $\phi_F = 0.53$.

The main spectroscopic data of both FNPs at pH8.0 are summarized in **Table 1**. Compared to red-BDPMA in toluene, a 6nm shift could be observed in FNP_{Red}'s emission as well a decrease of the fluorescence quantum yield $\phi_F = 0.25$, which is consistent with BODIPY aggregation-caused quenching. A similar trend was previously observed for this type of FNP with a green-emitting BODIPY³⁴. FNP_{Red} were also studied at various pH. All the absorbance and emission spectra are

shown in **Figure S1** and clearly demonstrate that both their absorbance and emission intensity are insensitive to the pH. The number of red-BDPMA per particle was evaluated by eq. S5 using absorption and NTA results. It was found to be approximately 4400, which is similar to our previous results³⁴.

Table 1. Spectroscopic and size data of red-BDPMA in toluene, FAM in 0.1M NaOH solution and FNPs in water (citrate-phosphate buffer, 0.1M, pH8.0)

Sample	$\lambda_{\text{abs}} (\epsilon)$ nm ($M^{-1}cm^{-1}$)	λ_{em} nm	ϕ_F^a	$N_{\text{red-BDPMA}}^b$	N_{FAM}^c	B^d $\times 10^{-7}(M^{-1}cm^{-1})$	$Dh \pm 2$ nm
red-BDPMA	558 (52 600)	600	0.53*				
FAM	490 (44 000)	515	0.65 [#]				
FNP _{Red}	558	606	0.25*	4400	-	0.7	70
FNP _{Red-FA}	497, 558	518, 607	0.35 [#]	4400	2100	4.1	70

^a Fluorescence quantum yield, given with 10% error, [#] Rhodamine 6g in ethanol ($\phi_F=0.94$) as reference, ^{*} Sulforhodamine in ethanol ($\phi_F=0.95$) as reference³⁹. ^b average number of red-BDPMA per nanoparticle, calculated using eq.S5 ^c average number of grafted FAM per nanoparticle, calculated using eq.S6 ^d B: Fluorescence Brightness when samples are excited at 488nm, calculated using eq.S7 for FNP_{Red} and eq. S8 for FNP_{Red-FA}.

As a control, both excitation and emission spectra of fluoresceinamide (5-acetamidofluorescein, FAM) were recorded at various pH (**Figure S2**). At pH 8.0, a 490nm excitation band was observed when the emission was fixed at 515nm. A 515nm emission band was observed when excitation was set at 488nm. Both bands are consistent with the anionic form of fluorescein²³. When pH was

decreased, as expected, both excitation and emission bands decreased. Fitting of the fluorescence intensities as a function of pH with the modified Henderson-Hasselbach eq. S1 gives $pK_a=6.4$.

The spectroscopic properties of FNP_{Red-FA} were first characterized at pH 8.0 (**Figure 2**). The FNP_{Red-FA} 's absorption spectrum features two bands, one at 497nm and the other at 558nm corresponding to FAM and red-BDPMA chromophores respectively. Similarly, the fluorescence emission spectrum recorded upon excitation at 488nm, shows two bands: one at 518nm, and the other at 607nm corresponding to FAM and red-BDPMA, respectively. The band position of red-BDPMA showed no difference between FNP_{Red} and FNP_{Red-FA} , which demonstrates that its spectroscopic properties are not affected by FAM grafting.

Compared to FAM in aqueous solution at pH 8.0, a 7nm red-shift appeared in the absorbance of FNP_{Red-FA} , and a 3nm red-shift in emission, which might be attributed to aggregation⁴⁰. The relative number of FAM compared to red-BDPMA was estimated by eq. S6 from the absorption spectrum at pH 8.0 (spectrum recorded with integrating sphere, **Figure S4**, and respective molecular extinction coefficients $\epsilon_{red-BDPMA}(558)=52600\text{ cm}^{-1}\text{M}^{-1}$ and $\epsilon_{FAM}(490)=44000\text{ cm}^{-1}\text{M}^{-1}$). A 0.48 FAM per red-BDPMA ratio was found. From this ratio and the previously estimated number of red-BDPMA per FNP, the number of FAM per particle was evaluated at approximately 2100. Assuming that FAM are homogeneously distributed on the FNPs surface, the mean distance between FAM could be estimated at roughly 27Å (eq. S9). There is thus a possibility to form weak FAM aggregates on the surface that leads to the observed bands shift in absorption and emission.

The global fluorescence quantum yield of FNP_{Red-FA} is 35% at pH 8.0. It is higher than FNP_{Red} which is due to the contribution of the 2 chromophores red-BDPMA and FAM. Concomitantly the FNP brightness at 490nm (excitation wavelength) increased from $B=0.7\times 10^7\text{ M}^{-1}\text{cm}^{-1}$ in FNP_{Red} to

$B = 4.1 \times 10^7 \text{ M}^{-1} \text{ cm}^{-1}$ in $\text{FNP}_{\text{Red-FA}}$, providing super-bright FNP as essential tools for efficient bioimaging⁴¹.

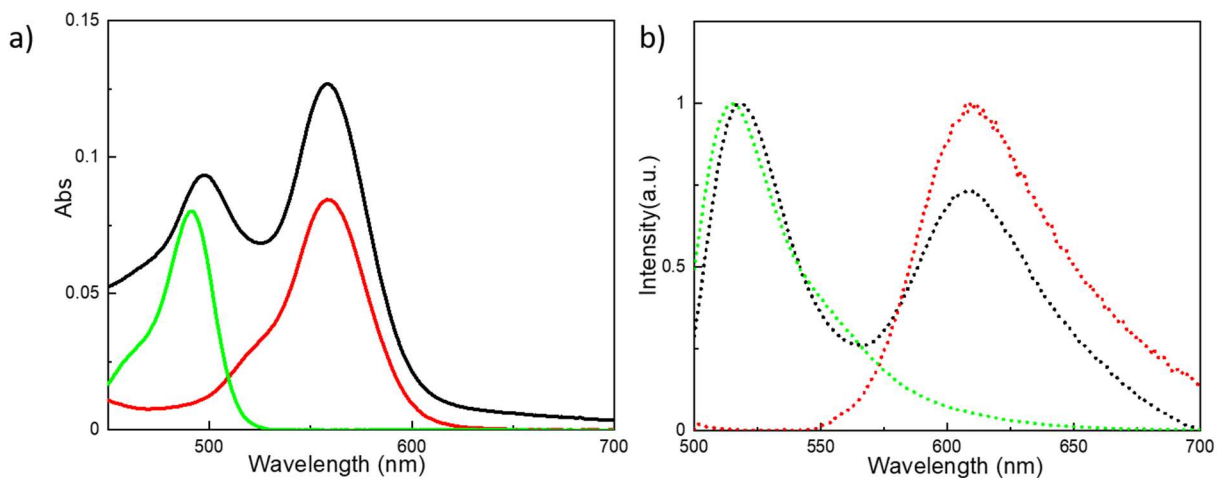


Figure 2. a) Absorption and b) normalized fluorescence emission spectra ($\lambda_{\text{ex}} = 488 \text{ nm}$) of FNP_{Red} (red), $\text{FNP}_{\text{Red-FA}}$ (black) and Fam (green) in citrate-phosphate buffer (0.1 M) at $\text{pH} = 8.0$

pH dependence of $\text{FNP}_{\text{Red-FA}}$ spectroscopic properties was then studied (**Figure 3**). The red-BDPMA absorption band at 558 nm was constant, while the FAM band at 497 nm decreased when pH was lowered from 8.0 to 5.0. Accordingly, both red-BDPMA and FAM emission bands decreased in the same pH range. The $\alpha_{518/607}$ which is the fluorescence intensities ratio at 518 and 607 nm (FAM vs. red-BDPMA) was evaluated (**Figure 3c**). It changed from 1.5 to 0.3 from pH 8.0 to 5.0. The curve $\alpha_{518/607}$ as a function of pH was fitted with the Henderson-Hasselbach equation (eq. S1) and gave a $\text{pK}_a = 6.5 \pm 0.1$ which is close to the value of fluorescein ($\text{pK}_a = 6.4$)²³. Spectra normalization on the red-BDPMA band does not affect pK_a determination (**Figure S3**).

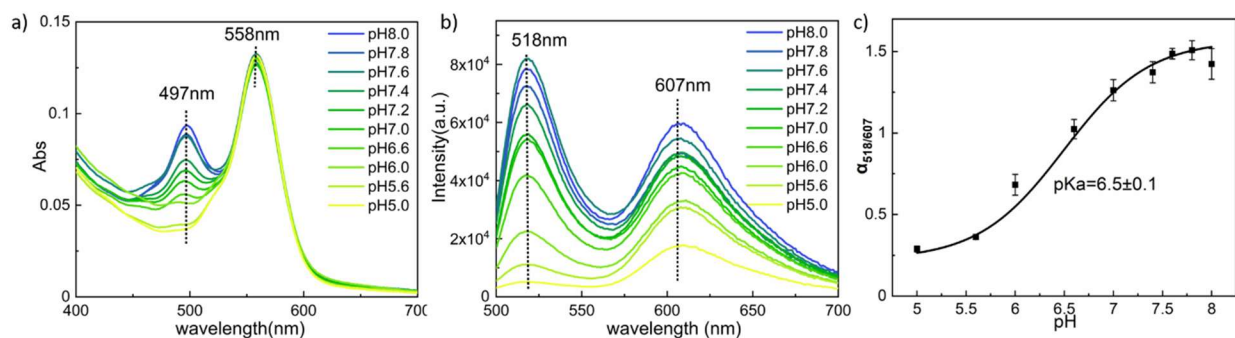


Figure 3. a) Absorbance spectra and b) Fluorescence emission spectra ($\lambda_{ex}=488\text{nm}$) of $\text{FNP}_{\text{Red-FA}}$ at various pH (citrate-phosphate buffer (0.1M) ranging from pH 8.0 to 5.0); c) Fluorescence intensity ratio of $\alpha_{518/607}$ (FAM/ red-BDPMA) as a function of pH, $pK_a=6.5\pm 0.1$ (fit with Henderson-Hasselbach equation)

The respective spectroscopic properties of FAM and red-BDPMA open the possibility of energy transfer between them where FAM is the energy donor while red-BDPMA is the acceptor (**Figure S5**). Since the red-BDPMA has the same microenvironment within FNP_{Red} and $\text{FNP}_{\text{Red-FA}}$, we selected a calculation based on its fluorescence emission spectra modulation to estimate the FRET efficiency⁴². FNP_{Red} with red-BDPMA only in the particle's core provides the data for the acceptor in the absence of the donor. Fluorescence spectra of the $\text{FNP}_{\text{Red-FA}}$ and FNP_{Red} suspensions that have the same concentration in red-BDPMA as controlled by the same absorbance at 558 nm (see insets in **Figure 4**) were recorded after excitation at $\lambda_{ex}=488\text{ nm}$ where the donor absorbs predominantly (**Figure 4**). At pH 8.0 (**Figure 4a**), FNP_{Red} displays a weak emission in the absence of the donor. However, the red-BDPMA displays an intense emission band in $\text{FNP}_{\text{Red-FA}}$. At pH 5.0 (**Figure 4b**), a similar FNP_{Red} emission is obtained but the red-BDPMA displays less pronounced emission enhancement in $\text{FNP}_{\text{Red-FA}}$. Such emission increase at $\lambda_{em}=607\text{nm}$ could either come from an overlap of the red-BDPMA emission with the FAM one or energy transfer

from the FAM to the red-BDPMA. To discriminate between these two hypotheses fluorescence emission of molecular FAM was recorded in both pH conditions (dotted spectra in **Figure 4**). It clearly appears that it has a minimal contribution at 607nm (red vertical lines) that cannot account for the observed enhancement (grey rectangles). Energy transfer efficiency is usually calculated according to eq. S13 in the absence of donor emission⁴³. However, in our case, we modified the formula according to eq. S14 to take into account the contribution of FAM emission. The transfer efficiency could be evaluated at 36% at pH 8.0 and 18% at pH 5.0. The efficiency dependency on pH comes from FAM donor fluorescence quantum yield variation (65% at pH 8.0 and 26% at pH 5.0, see SI for detailed discussion).

Using fluorescence quantum yield of molecular FAM at pH 8.0 (65%) Förster radius between FAM and red-BDPMA can be estimated at 51 Å with eq. S12. Subsequently, with eq. S11, a 56 Å donor-acceptor distance (r) was calculated. A copolymer chain made of acrylic acid and methyl methacrylate that mimics the hydrophilic shell of the FNP and bearing FAM and red-BDPMA at each end was optimized at PM6 level (**Figure S7**). The calculated distance between the two chromophores is 65 Å and represents the theoretical maximum distance between the two chromophores. The 56 Å donor-acceptor distance calculated with the FRET model indicates that the FA amine reacts more predominantly on the acrylic acids along the hydrophilic block rather than exclusively with the terminal carboxylic acid. This result sustains our hypothesis of an energy transfer between FAM and red-BDPMA that explains the observed acceptor fluorescence enhancement (I_{FRET} in **Figure 4**).

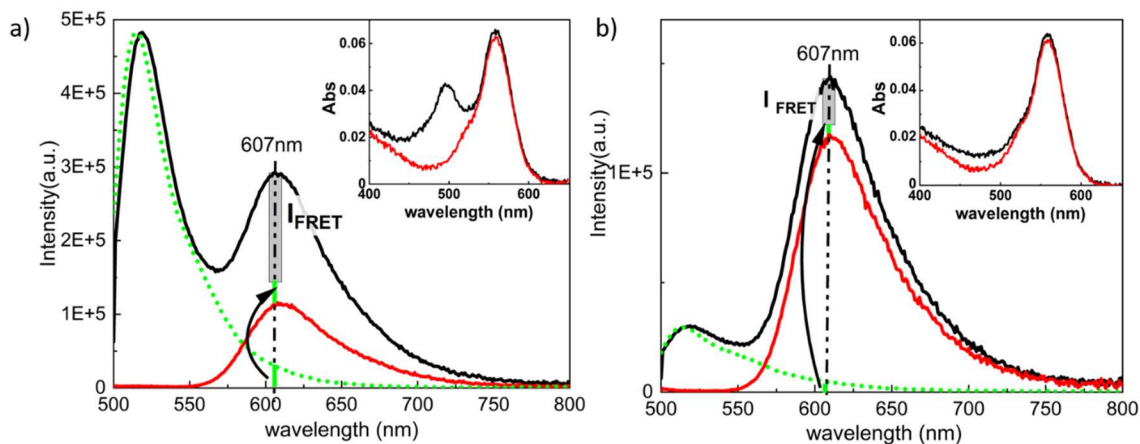
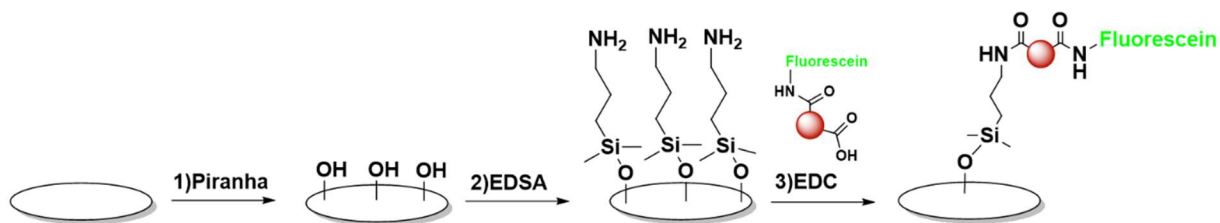


Figure 4. Superimposition of FNP_{Red-FA} (black) , FNP_{Red} (red) and normalized FAM (green) emission spectrum ($\lambda_{ex}=488\text{nm}$) for donor emission correction at acceptor wavelength: a) at pH 8.0, b) at pH 5.0; insets display the recorded absorption spectra of FNP_{Red-FA} and FNP_{Red}, green lines represent the contribution of FAM to the emission at 607 nm, the dotted line are the fluorescence emission intensities of red-BDPMA in the absence of the donor and I_{FRET} (grey rectangle) is the acceptor's fluorescence emission increase in the presence of donor

In summary, FNP_{Red-FA} is a ratiometric pH-sensitive platform where FRET occurs and is pH-dependent. The platform was then immobilized on the glass to prepare a reusable pH sensor.

Surface functionalization with FNP_{Red-FA} and Characterization

As preliminary results towards a future portable device, we immobilized the FNPs onto glass slides (**Scheme 1**). Glass slides were activated by a fresh piranha solution prior to silanization. We selected 3-(Ethoxydimethylsilyl) propylamine (EDSA) as the silanizing reagent and used the vapor deposition method to get a good monolayer formation^{35,36}. The FNP_{Red-FA} were further grafted on the silanized glass surface through peptide coupling using similar conditions as for FA (see materials and methods for details).



Scheme 1. FNP_{Red-FA} grafted surface preparation

The silanized surfaces were characterized by XPS. As shown in **Figure 5** left (C1s), taking potassium as a reference, only traces of carbon are detected on the surface after fresh piranha etching. This shows that most impurities and contaminants were removed from the surface. After silanization, the total carbon percentage increased from 0.73% to 9.1%, mainly due to $\text{-}\underline{\text{C}}\text{-NH}$ and $\text{-}\underline{\text{C}}\text{-(C, H)}$ bonds. The N1s band (**Figure 5** right) includes two contributions: a component at 399.8 eV attributed to amine groups [$\text{C-}\underline{\text{N}}\text{H}_2$] and a component at 401.5 eV due to protonated amines $\text{C-}\underline{\text{N}}\text{H}^{3+}$. Both components are obviously increased after silanization.

The amine density on the surface was determined by a colorimetric method based on the reversible complexation of the Coomassie brilliant blue (CBB) dye ($\lambda_{\text{abs}}=610\text{nm}$), assisted with UV-visible measurements (protocol of the method given in SI). The amine density in our case is $5.48 (\pm 0.50)$ chains per nm^2 , which is higher than reported silanized glass surfaces with other aminosilanes such as APTES^{44,45} and APDMES⁴⁶. The higher density of amine demonstrates a higher yield of silanization with the selected method.

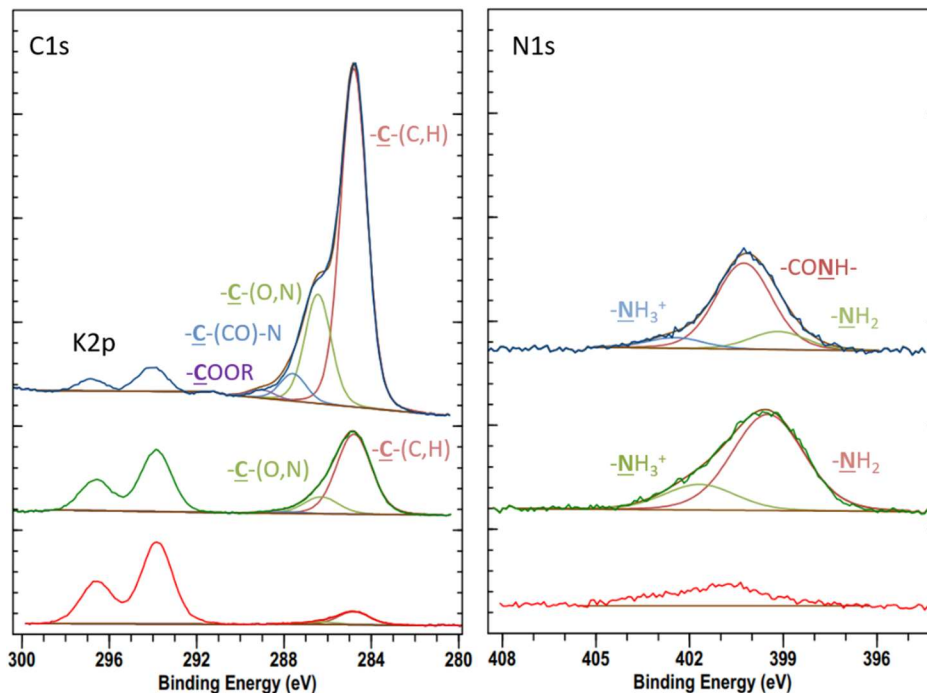


Figure 5. XPS Carbon (left) and nitrogen (right) windows of the glass slides after different treatments: bottom: glass after piranha activation; middle: surface after silanization; top: surface after FNP_{Red-FA} grafting.

XPS analysis of NPs grafted surface (**Figure 5**) shows that the carbon proportion further increases from 9.1% to 39.0% upon peptide coupling of FNP on the silanized surface. From the carbon band decomposition, the percentage of amide bonds ([$-\text{C}-(\text{O}, \text{N})$] and [$-\text{C}-(\text{C}=\text{O})-\text{NH}$]) is increased. Simultaneously in the Nitrogen window, a contribution from $(\text{C}=\text{O})-\text{NH}$ single bonds appears. These results prove that the FNP are covalently linked to the silanized glass slide.

The morphology of the surface grafted with NPs was investigated by AFM and SEM (**Figure 6**). SEM gives global information about the surface topography since it screens a larger area than AFM (see **Figure S9** $96 \mu\text{m}^2$ for SEM, much larger compared to $5 \times 5 \mu\text{m}^2$ for AFM). SEM images are helpful to investigate nanoparticle distribution while AFM gives better insight into nanoparticles' shape and layer thickness.

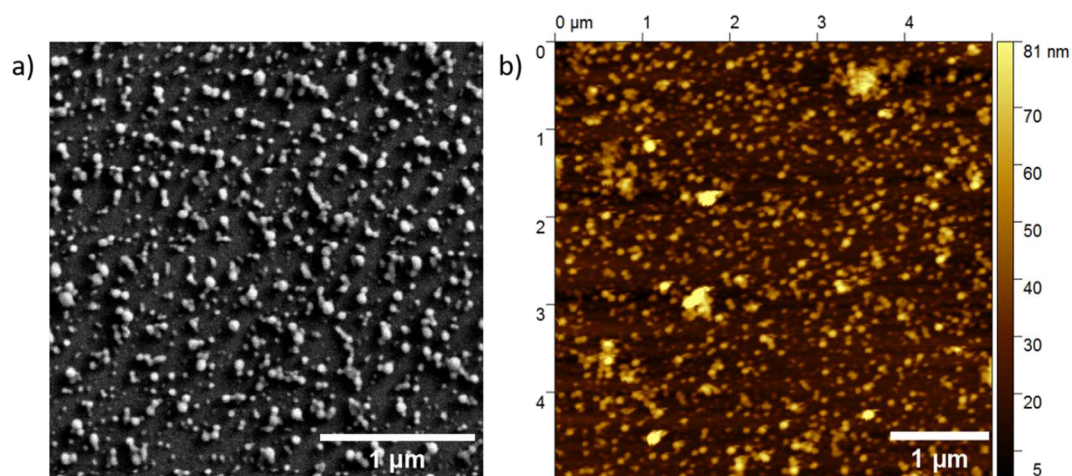


Figure 6. a) SEM and b) AFM (tapping mode) images of FNP_{Red-FA} grafted on a glass slide

The SEM images show randomly distributed particles on the surface. The average diameter of the nanoparticles is 61 ± 16 nm which is close to the diameter measured in suspension (see **Table 1**). Similar particles size was also observed through the AFM experiment. AFM images confirm the average height of the particle layer as 67 ± 16 nm. From both SEM and AFM images, we can estimate a similar nanoparticle coverage: $16 \pm 2\%$ and $14 \pm 2\%$ respectively. The FNP's density could then be calculated to be 0.00005 particles per nm^2 , which is much lower than the amine density which is about 5.5 functions per nm^2 .

Spectroscopic characterization of the surfaces and Bacterial growth monitoring.

Emission spectra of the grafted surfaces (**Figure S10**) were monitored by confocal microscopy in the dry state and at pH 7.0 (citrate-phosphate buffer, 0.1M). Dual emission spectra are obtained only when the surface is covered with buffer. Fluorescein signal is completely lost in the dry state. The maximum emission bands with buffer are found at 520nm for FAM and 600 nm for red-BDPMA which is consistent with bands position in suspension. In the dry state, fluorescein signal loss is likely due to polymer chain folding causing aggregation-induced self-quenching of the dye.

A similar phenomenon has already been observed by Maciej's group. Fluorescein-modified polymer chains emission was quenched due to aggregation upon solvent evaporation or in a non-polar solvent^{47,48}. In our case, after buffer addition, the distance between FAM molecules increased with the polymer chain unfolding leading to partial fluorescence recovery. Another hypothesis for the loss of the FAM signal could be the FNPs microenvironment change from suspension to surface. On the surface, sensitive chromophores are surrounded by a large amount of amines/ammonium ions, which leads to an ionic strength change that might contribute to some extent to the fluorescence quenching⁴⁹.

Although the FAM relative intensity is reduced compared to suspension, grafted FNP_{Red-FA} still display dual emission and preserve pH sensitivity in an aqueous environment as demonstrated by ratiometric pH calibration of the surfaces (**Figure 7**). Fluorescence emission spectra of FNP_{Red-FA} surfaces were measured at different pH, ranging from pH 5.0 to 7.6 under confocal microscope. Spectra of the surface recorded with the microscope always came up with signal fluctuation either due to low signal-to-noise ratio or slight microscope stage drift during buffer change (raw spectra are given in **Figure S11**).

The fluorescence intensity of FAM at 520nm was gradually weakened with decreasing pH. Thus the ratiometric behavior is preserved from suspension to glass surfaces. Four independent experiments were done with different surfaces from the same batch (data are presented in **Figure S11, S12**). Ratio variability can be observed which is likely due to surface grafting heterogeneities and instrument background noise. Since normalization does not affect pKa determination as formerly demonstrated with suspension, normalized spectra are provided (**Figure 7a**). The $\alpha_{520/600}$ related ratio was plotted as a function of pH (**Figure 7b**). Henderson Hasselbach fitting gives $pK_a=6.4\pm 0.1$ ($R^2=0.99$) which is close to the pKa determined in suspension (**Figure 3**). Compared

with the calibration curve obtained for FNPs in suspension, the grafted surface contrast between pH 5.0 and 7.0 is lower. It might result from a fluorescein reduced signal coming from self-quenching.

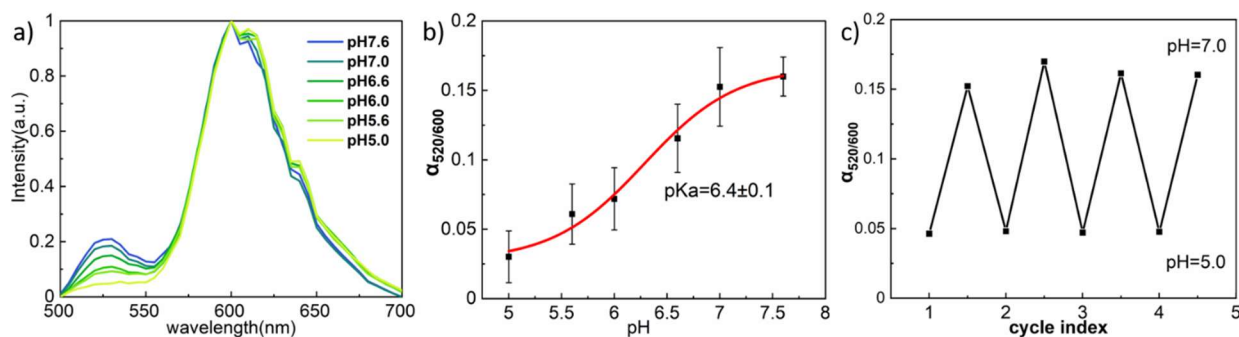


Figure 7. a) Normalized fluorescence emission spectra recorded with confocal microscope; b) pH calibration curve between pH 5.0-7.6; c) pH reversibility study of surface grafted FNP_{Red-FA} between pH 5.0-7.0

The reversibility of the surface sensitivity to pH was investigated by cycling the pH between 5.0 and 7.0 four times (**Figure 7c**). Good reversibility and robustness of the surface are obtained since no signal loss is detected.

The surfaces were tested to detect bacteria growth in a culture medium by pH monitoring. Bacteria's growth induces the production of acid metabolites such as lactic acid, and certain amino acids that decrease the surrounding environment's pH. With confocal microscope, bacteria growth could be followed through the bright channel (phase-contrast image, **Figure 8a**). It allows quantification of increasing bacteria number (**Table S3**). During the first hour, *E. coli* could be hardly detected, because of a too low bacteria density (most of them were floating in the medium). After 3h, there are too many bacteria to be counted with reliability and counting was successful in between. However, the emission spectra could be recorded from the initial time until 6h (**Figure**

8b). Fluorescence allows continuous monitoring over 360 min. The fluorescence intensity ratio was then calculated (**Table S3**) and decreases as of cell number increase (**Figure S15**). It could be converted to a pH value according to the calibration curve (**Figure 8c**). The pH of the medium decreases from pH 6.7 to 5.4 as bacteria grow. Such a result demonstrates that the ratiometric fluorescence monitoring is more sensitive than direct bacteria counting both at early and long time.

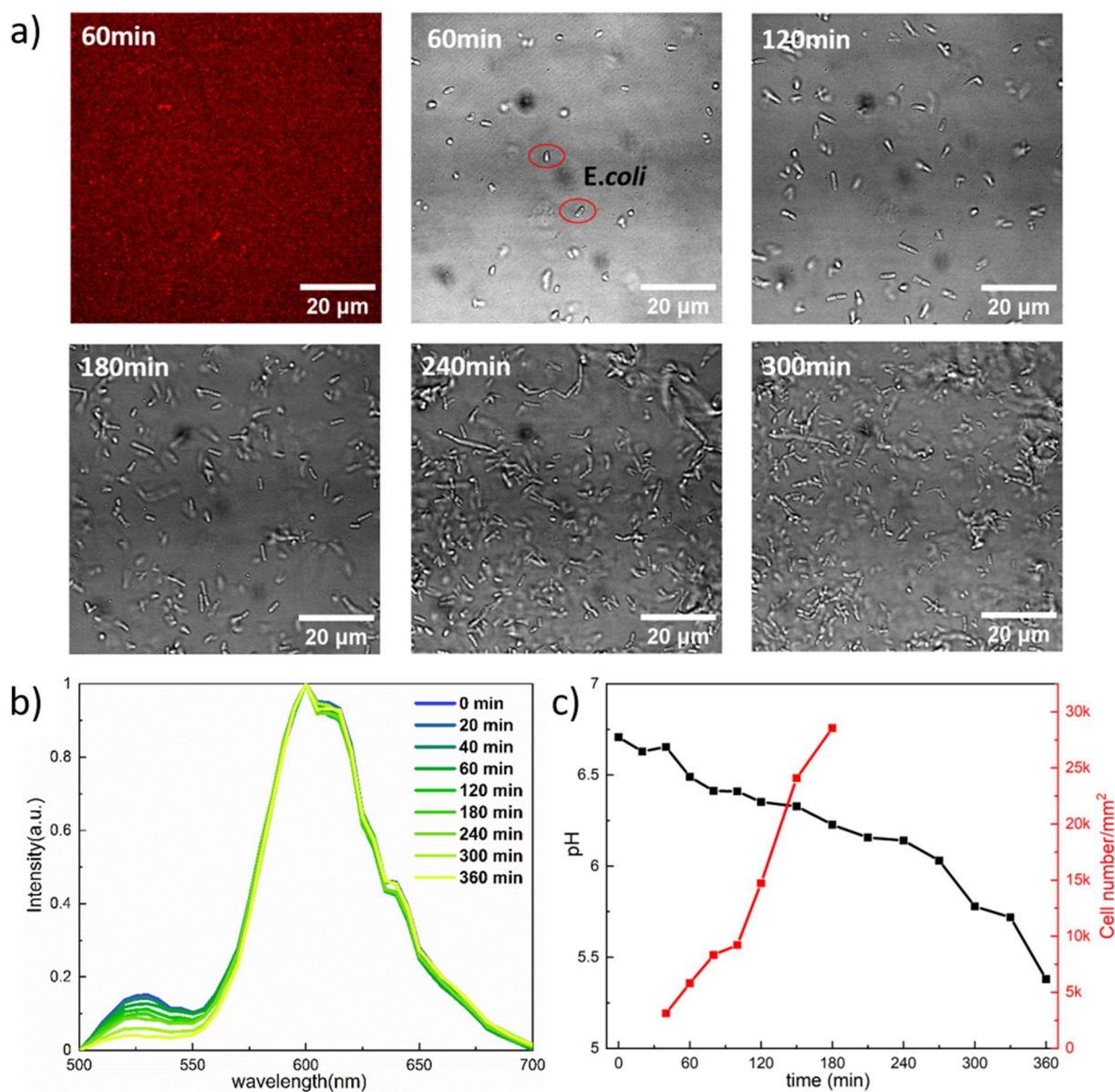


Figure 8. a) Fluorescent channel and bright channel of confocal microscope with bacterial growth observation during 300 min; b) Normalized fluorescence emission intensity spectra recorded

during bacterial growth; c) Calculated pH and bacteria count in observation zone ($82.01\mu\text{m} \times 82.01\mu\text{m}$)

Conclusion

In summary, we synthesized a red-emitting naphthalene-methacrylate BODIPY derivative that was further incorporated in fluorescent polymeric nanoparticles (FNP_{Red}) to prepare a platform for sensing. Fluoresceinamide, a pH-sensitive dye, was grafted on the FNP_{Red} 's outer shell. Ratiometric pH-sensitive $\text{FNP}_{\text{Red-FA}}$ were successfully obtained and characterized ($\text{pK}_a = 6.5$). A FRET-pH-dependent behavior has been demonstrated. The successful immobilization of such ratiometric $\text{FNP}_{\text{Red-FA}}$ onto silanized glass surface through covalent grafting was then shown. A good glass surface coverage was determined by AFM and SEM. The designed luminescent glass surface demonstrated its ability for reversible pH detection, with good reproducibility in the physiological range of 5.0-7.6. Moreover, with confocal spectral imaging, it was possible to monitor bacteria *E. coli* growth. Due to their extreme brightness ($4 \times 10^{-7} \text{ M}^{-1}\text{cm}^{-1}$), such a nanoparticle-based sensor is relatively easy to transpose to a point-of-care device⁵⁰: a surface covered with the dual colors FNPs is put in the presence of bacteria contaminated aqueous sample. Upon excitation by a blue LED (exc 450-490 nm) and after detection of the two fluorescence emissions that are sufficiently far apart to be de-coupled ($\sim 520 \text{ nm}$ and 610 nm) e.g. with the aid of a transportable spectrometer, the monitoring of bacterial growth should be allowed⁵¹. It would thus offer a more robust, transportable and easy-to-handle set-up. We are currently expanding the scope of our FNP platform by grafting other sensitive moieties to detect various types of pollutants.

ASSOCIATED CONTENT

Supporting Information

Molecular structure, synthetic details and characterization of chromophores with nanoparticles; Absorption and fluorescence emission properties of FAM; Spectroscopic characterization of FNPs; Förster resonance energy transfer (FRET) calculation; Surface characterization with amine density measurement alongside with surface pH calibration spectra.

AUTHOR INFORMATION

Corresponding Author

*E-mail: rachel.meallet-renault@universite-paris-saclay.fr

Present Addresses

¹ Université Paris-Saclay, Institut des Sciences Moléculaires d'Orsay (ISMO), CNRS, 91400, Orsay, France

² Université Paris-Saclay, ENS Paris-Saclay, CNRS, PPSM, 91190, Gif-sur-Yvette, France

³ Université Bordeaux, CNRS, Bordeaux INP, ISM, UMR 5255, F-33400 Talence, France

Author Contributions

The manuscript was written through contributions of all authors. All authors have given approval to the final version of the manuscript.

Funding Sources

Financial support for this work was provided by the CNRS (Centre National de la Recherche Scientifique) of France, Conseil régional d'île de France DIM Nano'K, and Université Paris-Saclay. Miaobo PAN acknowledges support from China Scholarship Council (CSC, N°201808320426). This work was supported by a grant from the Ministère de l'Éducation Nationale, de l'Enseignement Supérieur et de la Recherche, Université Paris Saclay, for Gabriela Moran's PhD thesis (ED 2MIB No. 571).

Notes

The authors have no competing interests to declare that are relevant to the content of this article.

ACKNOWLEDGMENT

We are grateful to Dr. Diana Dragoe for the XPS experiments, François Brisset for SEM experiments, from ICMMO. We are grateful to Dr Bianca Sclavi for her suggestions about biological evaluation and Pr Antoine Pallandre for scientific discussion on surface silanization.

ABBREVIATIONS

AA, acrylic acid; BODIPY, boron dipyrromethene; FAm, fluoresceinamide; FNP, fluorescent nanoparticle; FRET, Förster resonance energy transfer; PEOA, poly-(ethylene oxide) acrylate; RAFT, reversible addition–fragmentation chain-transfer; red-BDPMA, red-emitting naphthalene-methacrylate BODIPY derivative.

REFERENCES

- (1) Akter, T.; Jhohura, F. T.; Akter, F.; Chowdhury, T. R.; Mistry, S. K.; Dey, D.; Barua, M. K.; Islam, M. A.; Rahman, M. Water Quality Index for Measuring Drinking Water Quality in Rural Bangladesh: A Cross-Sectional Study. *J. Heal. Popul. Nutr.* **2016**, *35* (1), 4. <https://doi.org/10.1186/s41043-016-0041-5>.
- (2) Jeevarajan, A. S.; Vani, S.; Taylor, T. D.; Anderson, M. M. Continuous PH Monitoring in a Perfused Bioreactor System Using an Optical PH Sensor. *Biotechnol. Bioeng.* **2002**, *78* (4), 467–472. <https://doi.org/10.1002/bit.10212>.
- (3) Sun, H.; Qing, T.; He, X.; Shangguan, J.; Jia, R.; Bu, H.; Huang, J.; Wang, K. Rapid

- Synthesis of Au/Ag Bimetallic Nanoclusters with Highly Biochemical Stability and Its Applications for Temperature and Ratiometric PH Sensing. *Anal. Chim. Acta* **2019**, *1070*, 88–96. <https://doi.org/10.1016/j.aca.2019.04.029>.
- (4) Ghoneim, M. T.; Nguyen, A.; Dereje, N.; Huang, J.; Moore, G. C.; Murzynowski, P. J.; Dagdeviren, C. Recent Progress in Electrochemical PH-Sensing Materials and Configurations for Biomedical Applications. *Chem. Rev.* **2019**, *119* (8), 5248–5297. <https://doi.org/10.1021/acs.chemrev.8b00655>.
- (5) Mane, S. R.; Sathyan, A.; Shunmugam, R. Biomedical Applications of PH-Responsive Amphiphilic Polymer Nanoassemblies. *ACS Appl. Nano Mater.* **2020**, *3* (3), 2104–2117. <https://doi.org/10.1021/acsanm.0c00410>.
- (6) Fuertes, G.; Soto, I.; Carrasco, R.; Vargas, M.; Sabatin, J.; Lagos, C. Intelligent Packaging Systems: Sensors and Nanosensors to Monitor Food Quality and Safety. *J. Sensors* **2016**, *2016*, 4046061. <https://doi.org/10.1155/2016/4046061>.
- (7) Pounds, K.; Jairam, S.; Bao, H.; Meng, S.; Zhang, L.; Godinez, S.; Savin, D. A.; Pelletier, W.; Correll, M. J.; Tong, Z. Glycerol-Based Dendrimer Nanocomposite Film as a Tunable PH-Sensor for Food Packaging. *ACS Appl. Mater. Interfaces* **2021**, *13* (19), 23268–23281. <https://doi.org/10.1021/acсами.1c05145>.
- (8) Luchese, C. L.; Sperotto, N.; Spada, J. C.; Tessaro, I. C. Effect of Blueberry Agro-Industrial Waste Addition to Corn Starch-Based Films for the Production of a PH-Indicator Film. *Int. J. Biol. Macromol.* **2017**, *104*, 11–18. <https://doi.org/10.1016/j.ijbiomac.2017.05.149>.
- (9) Sinha, S.; Pal, T. A Comprehensive Review of FET-Based PH Sensors: Materials,

- Fabrication Technologies, and Modeling. *Electrochem. Sci. Adv.* **2021**, *n/a* (n/a), 2100147. <https://doi.org/10.1002/elsa.202100147>.
- (10) Korostynska, O.; Arshak, K.; Gill, E.; Arshak, A. State Key Laboratory of Nonlinear Mechanics (LNM), Institute of Mechanics, Chinese Academy of Sciences, Beijing 100080, China. *Sensors (Basel)*. **2007**, *7* (12), 3027–3042. <https://doi.org/10.3390/s7123027>.
- (11) Miao, Q.; Pu, K. Organic Semiconducting Agents for Deep-Tissue Molecular Imaging: Second Near-Infrared Fluorescence, Self-Luminescence, and Photoacoustics. *Adv. Mater.* **2018**, *30* (49), 1801778. <https://doi.org/10.1002/adma.201801778>.
- (12) Shamsipur, M.; Barati, A.; Nematifar, Z. Fluorescent PH Nanosensors: Design Strategies and Applications. *J. Photochem. Photobiol. C Photochem. Rev.* **2019**, *39*, 76–141. <https://doi.org/10.1016/j.jphotochemrev.2019.03.001>.
- (13) Huang, X.; Song, J.; Yung, B. C.; Huang, X.; Xiong, Y.; Chen, X. Ratiometric Optical Nanoprobes Enable Accurate Molecular Detection and Imaging. *Chem. Soc. Rev.* **2018**, *47* (8), 2873–2920. <https://doi.org/10.1039/C7CS00612H>.
- (14) Steinegger, A.; Wolfbeis, O. S.; Borisov, S. M. Optical Sensing and Imaging of PH Values: Spectroscopies, Materials, and Applications. *Chem. Rev.* **2020**, *120* (22), 12357–12489. <https://doi.org/10.1021/acs.chemrev.0c00451>.
- (15) Alam, A. U.; Qin, Y.; Nambiar, S.; Yeow, J. T. W.; Howlader, M. M. R.; Hu, N.-X.; Deen, M. J. Polymers and Organic Materials-Based PH Sensors for Healthcare Applications. *Prog. Mater. Sci.* **2018**, *96*, 174–216. <https://doi.org/10.1016/j.pmatsci.2018.03.008>.
- (16) Lian, Y.; Zhang, W.; Ding, L.; Zhang, X.; Zhang, Y.; Wang, X. Chapter 8 - Nanomaterials

- for Intracellular PH Sensing and Imaging. In *Micro and Nano Technologies*; Wang, X., Chen Environmental and Energy Applications, X. B. T.-N. N. for B., Eds.; Elsevier, 2019; pp 241–273. <https://doi.org/10.1016/B978-0-12-814497-8.00008-4>.
- (17) Li, Y.-Y.; Cheng, H.; Zhu, J.-L.; Yuan, L.; Dai, Y.; Cheng, S.-X.; Zhang, X.-Z.; Zhuo, R.-X. Temperature- and PH-Sensitive Multicolored Micellar Complexes. *Adv. Mater.* **2009**, *21* (23), 2402–2406. <https://doi.org/https://doi.org/10.1002/adma.200803770>.
- (18) Yao, Q.; Lu, S.; Lin, F.; Zhao, T.; Zhao, L.; Chen, X. A Co-Precipitation Strategy for Making a Ratiometric PH Nanosensor for Intracellular Imaging. *Sensors Actuators B Chem.* **2017**, *250*, 484–490. <https://doi.org/10.1016/j.snb.2017.04.097>.
- (19) Wolfbeis, O. S. An Overview of Nanoparticles Commonly Used in Fluorescent Bioimaging. *Chem. Soc. Rev.* **2015**, *44* (14), 4743–4768. <https://doi.org/10.1039/C4CS00392F>.
- (20) Smith, B. R.; Gambhir, S. S. Nanomaterials for In Vivo Imaging. *Chem. Rev.* **2017**, *117* (3), 901–986. <https://doi.org/10.1021/acs.chemrev.6b00073>.
- (21) Wencel, D.; Abel, T.; McDonagh, C. Optical Chemical PH Sensors. *Anal. Chem.* **2014**, *86* (1), 15–29. <https://doi.org/10.1021/ac4035168>.
- (22) Han, J.; Burgess, K. Fluorescent Indicators for Intracellular PH. *Chem. Rev.* **2010**, *110* (5), 2709–2728. <https://doi.org/10.1021/cr900249z>.
- (23) Sjöback, R.; Nygren, J.; Kubista, M. Absorption and Fluorescence Properties of Fluorescein. *Spectrochim. Acta Part A Mol. Biomol. Spectrosc.* **1995**, *51* (6), L7–L21. [https://doi.org/10.1016/0584-8539\(95\)01421-P](https://doi.org/10.1016/0584-8539(95)01421-P).
- (24) Le Guern, F.; Mussard, V.; Gaucher, A.; Rottman, M.; Prim, D. Fluorescein Derivatives as

- Fluorescent Probes for PH Monitoring along Recent Biological Applications. *Int. J. Mol. Sci.* **2020**, *21* (23), 1–23. <https://doi.org/10.3390/ijms21239217>.
- (25) Squeo, B. M.; Gregoriou, V. G.; Avgeropoulos, A.; Baysec, S.; Allard, S.; Scherf, U.; Chochos, C. L. BODIPY-Based Polymeric Dyes as Emerging Horizon Materials for Biological Sensing and Organic Electronic Applications. *Prog. Polym. Sci.* **2017**, *71*, 26–52. <https://doi.org/10.1016/j.progpolymsci.2017.02.003>.
- (26) Poddar, M.; Misra, R. Recent Advances of BODIPY Based Derivatives for Optoelectronic Applications. *Coord. Chem. Rev.* **2020**, *421*, 213462. <https://doi.org/10.1016/j.ccr.2020.213462>.
- (27) Loudet, A.; Burgess, K. BODIPY Dyes and Their Derivatives: Syntheses and Spectroscopic Properties. *Chem. Rev.* **2007**, *107* (11), 4891–4932. <https://doi.org/10.1021/cr078381n>.
- (28) Kowada, T.; Maeda, H.; Kikuchi, K. BODIPY-Based Probes for the Fluorescence Imaging of Biomolecules in Living Cells. *Chem. Soc. Rev.* **2015**, *44* (14), 4953–4972. <https://doi.org/10.1039/C5CS00030K>.
- (29) Li, F.-Z.; Yin, J.-F.; Kuang, G.-C. BODIPY-Based Supramolecules: Construction, Properties and Functions. *Coord. Chem. Rev.* **2021**, *448*, 214157. <https://doi.org/https://doi.org/10.1016/j.ccr.2021.214157>.
- (30) Grazon, C.; Si, Y.; Placial, J.-P.; Rieger, J.; Méallet-Renault, R.; Clavier, G. Core–Shell Polymeric Nanoparticles Comprising BODIPY and Fluorescein as Ultra-Bright Ratiometric Fluorescent PH Sensors. *Photochem. Photobiol. Sci.* **2019**, *18* (5), 1156–1165.

<https://doi.org/10.1039/C8PP00457A>.

- (31) Wang, T.; Hong, T.; Huang, Y.; Su, H.; Wu, F.; Chen, Y.; Wei, L.; Huang, W.; Hua, X.; Xia, Y.; Xu, J.; Gan, J.; Yuan, B.; Feng, Y.; Zhang, X.; Yang, C.-G.; Zhou, X. Fluorescein Derivatives as Bifunctional Molecules for the Simultaneous Inhibiting and Labeling of FTO Protein. *J. Am. Chem. Soc.* **2015**, *137* (43), 13736–13739. <https://doi.org/10.1021/jacs.5b06690>.
- (32) Grazon, C.; Rieger, J.; Méallet-Renault, R.; Clavier, G.; Charleux, B. One-Pot Synthesis of Pegylated Fluorescent Nanoparticles by RAFT Miniemulsion Polymerization Using a Phase Inversion Process. *Macromol. Rapid Commun.* **2011**, *32* (9–10), 699–705. <https://doi.org/10.1002/marc.201100008>.
- (33) Grazon, C.; Rieger, J.; Beaunier, P.; Méallet-Renault, R.; Clavier, G. Fluorescent Core–Shell Nanoparticles and Nanocapsules Using Comb-like Macromolecular RAFT Agents: Synthesis and Functionalization Thereof. *Polym. Chem.* **2016**, *7* (25), 4272–4283. <https://doi.org/10.1039/C6PY00646A>.
- (34) Grazon, C.; Rieger, J.; Méallet-Renault, R.; Charleux, B.; Clavier, G. Ultrabright Fluorescent Polymeric Nanoparticles Made from a New Family of BODIPY Monomers. *Macromolecules* **2013**, *46* (13), 5167–5176. <https://doi.org/10.1021/ma400590q>.
- (35) Asenath Smith, E.; Chen, W. How to Prevent the Loss of Surface Functionality Derived from Aminosilanes. *Langmuir* **2008**, *24* (21), 12405–12409. <https://doi.org/10.1021/la802234x>.
- (36) Pallandre, A.; Glinel, K.; Jonas, A. M.; Nysten, B. Binary Nanopatterned Surfaces Prepared

- from Silane Monolayers. *Nano Lett.* **2004**, *4* (2), 365–371.
<https://doi.org/10.1021/nl035045n>.
- (37) Trofimov, B. A.; Mikhaleva, A. I.; Schmidt, E. Y.; Sobenina, L. N. CHAPTER 7 - Pyrroles and N-Vinylpyrroles from Ketones and Acetylenes: Recent Strides. *Adv. Heterocycl. Chem.* **2010**, *99*, 209–254. [https://doi.org/0.1016/S0065-2725\(10\)09907-1](https://doi.org/0.1016/S0065-2725(10)09907-1).
- (38) Montalbetti, C. A. G. N.; Falque, V. Amide Bond Formation and Peptide Coupling. *Tetrahedron* **2005**, *61* (46), 10827–10852. <https://doi.org/10.1016/j.tet.2005.08.031>.
- (39) Brouwer, A. M. Standards for Photoluminescence Quantum Yield Measurements in Solution (IUPAC Technical Report). *Pure Appl. Chem.* **2011**, *83* (12), 2213–2228. <https://doi.org/10.1351/PAC-REP-10-09-31>.
- (40) Goncalves, S.; Castillo, J.; Fernandez, A.; Hung, J. Absorbance and Fluorescence Spectroscopy on the Aggregation Behavior of Asphaltene–Toluene Solutions. *Fuel* **2004**, *83* (13), 1823–1828. <https://doi.org/10.1016/j.fuel.2004.03.009>.
- (41) Reisch, A.; Klymchenko, A. S. Fluorescent Polymer Nanoparticles Based on Dyes: Seeking Brighter Tools for Bioimaging. *Small* **2016**, *12* (15), 1968–1992. <https://doi.org/10.1002/smll.201503396>.
- (42) Lakowicz, J. R. *Principles of Fluorescence Spectroscopy*; Springer, 2006. <https://doi.org/10.1007/s00216-007-1822-x>.
- (43) Valeur, B.; Berberan-Santos, M. N. *Molecular Fluorescence: Principles and Applications*; John Wiley & Sons, 2012. <https://doi.org/10.1002/9783527650002>.
- (44) Xiang, S.; Xing, G.; Xue, W.; Lu, C.; Lin, J.-M. Comparison of Two Different Deposition

- Methods of 3-Aminopropyltriethoxysilane on Glass Slides and Their Application in the ThinPrep Cytologic Test. *Analyst* **2012**, *137* (7), 1669–1673. <https://doi.org/10.1039/C2AN15983J>.
- (45) Wang, W.; Vaughn, M. W. Morphology and Amine Accessibility of (3-Aminopropyl) Triethoxysilane Films on Glass Surfaces. *Scanning J. Scanning Microsc.* **2008**, *30* (2), 65–77. <https://doi.org/10.1002/sca.20097>.
- (46) Yang, Z.; Chevolut, Y.; Gehin, T.; Dugas, V.; Xanthopoulos, N.; Laporte, V.; Delair, T.; Ataman-Önal, Y.; Choquet-Kastylevsky, G.; Souteyrand, E. Characterization of Three Amino-Functionalized Surfaces and Evaluation of Antibody Immobilization for the Multiplex Detection of Tumor Markers Involved in Colorectal Cancer. *Langmuir* **2013**, *29* (5), 1498–1509. <https://doi.org/10.1021/la3041055>.
- (47) Kopeć, M.; Tas, S.; Cirelli, M.; van der Pol, R.; de Vries, I.; Vancso, G. J.; de Beer, S. Fluorescent Patterns by Selective Grafting of a Telechelic Polymer. *ACS Appl. Polym. Mater.* **2019**, *1* (2), 136–140. <https://doi.org/10.1021/acsapm.8b00180>.
- (48) Tas, S.; Kopeć, M.; van der Pol, R.; Cirelli, M.; de Vries, I.; Bölükbas, D. A.; Tempelman, K.; Benes, N. E.; Hempenius, M. A.; Vancso, G. J. Chain End-Functionalized Polymer Brushes with Switchable Fluorescence Response. *Macromol. Chem. Phys.* **2019**, *220* (5), 1800537. <https://doi.org/10.1002/macp.201800537>.
- (49) Blom, H.; Hassler, K.; Chmyrov, A.; Widengren, J. Electrostatic Interactions of Fluorescent Molecules with Dielectric Interfaces Studied by Total Internal Reflection Fluorescence Correlation Spectroscopy. *Int. J. Mol. Sci.* **2010**, *11* (2), 386–406. <https://doi.org/10.3390/ijms11020386>.

- (50) Petryayeva, E.; Algar, W. R. Toward Point-of-Care Diagnostics with Consumer Electronic Devices: The Expanding Role of Nanoparticles. *RSC Adv.* **2015**, *5* (28), 22256–22282. <https://doi.org/10.1039/C4RA15036H>.
- (51) Gotor, R.; Tiebe, C.; Schlichka, J.; Bell, J.; Rurack, K. Detection of Adulterated Diesel Using Fluorescent Test Strips and Smartphone Readout. *Energy & Fuels* **2017**, *31* (11), 11594–11600. <https://doi.org/10.1021/acs.energyfuels.7b01538>.